NANO LETTERS

2007
Vol. 7, No. 9
2926−2930

Optical Transmission through Hexagonal Arrays of Subwavelength Holes in Thin Metal Films

G. Ctistis,*,† P. Patoka,† X. Wang,‡ K. Kempa,‡ and M. Giersig†

Nanoparticle Technology Department, Center of Advanced Studies and Research, 53175 Bonn, Germany, and Department of Physics, Boston College, Chestnut Hill, Massachusetts 02467-3811

Received June 1, 2007; Revised Manuscript Received July 30, 2007

ABSTRACT

We have studied the light transmission through hexagonal arrays of subwavelength holes in thin gold and aluminum films, varying the film thickness between 20 and 120 nm while the hole diameter as well as the interhole distance have been kept constant at ∼300 and ∼500 nm, respectively. The films were characterized by means of UV−vis spectroscopy and scanning near-field optical microscopy (SNOM).

The transmission properties of a subwavelength hole in a metal film have been under investigation since the first predictions by Bethe[1] in 1944. In an attempt to understand the transmission processes, which are essential in near-field optical microscopy, many theoretical[2−4] as well as experimental[5−8] studies had been carried out.

Extending the single hole to a periodic array of subwavelength holes in a metal film results in an extraordinary transmission through the film, as was shown by Ebbesen and co-workers.[9] This discovery has been followed by a large amount of theoretical[10−17] and experimental[18−24] work. Nowadays, the excitation of surface plasmons is widely accepted to be responsible for this enhanced transmission. Yet, the periodicity and the arrangement of the 2D lattice of the holes also play a significant role for the observed amount of maxima in the spectra.[25] By changing these structural parameters, it is possible to change the transmission properties to desired wavelength regions and therefore manipulate the light propagation through the film, the latter being the main aim of the field of plasmonics.[26]

In this work, we will present our experimental and theoretical investigations on light transmission through a hexagonal array of subwavelength holes in optically thin gold and aluminum films with thicknesses in the range between 20 and 120 nm.

The outline of the paper is as follows: A brief discussion on the experimental details will be followed by the discussion of the theoretical and experimental data. Finally, the conclusions will be summarized and an outlook on future experiments will be given.

Experimental Section. The films under study were prepared by using self-assembly lithography.[27] In our experiments, polystyrene (PS) latex spheres with a diameter of 470 nm (diluted in water) were dispersed in an ethanol−water solution and slowly applied to a water surface in a petri dish using a glass pipet. A reorientation of the spheres on the surface then formed a hexagonal closed-packed, defect-free monolayer of the spheres, which was deposited onto a clean sapphire substrate by evaporation of the water. Because this closed-packed structure prohibits the growth of a closed film, the diameter of the PS-spheres had been reduced to approximately 250 nm by means of reactive ion etching. Afterward, the obtained structure served as a mask for the evaporation of the metal films. The gold and aluminum thin films with thicknesses of 20, 50, and 120 nm, respectively, were deposited on top of a 2 nm thick Ti buffer layer by means of molecular-beam epitaxy at a base pressure of 10^{-7} mbar. Thereafter, the PS spheres were removed by thermal and chemical treatment, leaving the metal film with an array of ordered holes. The last step of the preparation included the cleaning and rinsing of the surface with propanol and drying under Ar flow.

The samples were routinely characterized with an UV−vis spectrometer (Varian) and under an atomic force microscope (AFM; Digital Instruments). The latter confirmed formation of large area defect-free arrays of subwavelength holes in the metal films. The near-field optical investigations were performed by using a combined AFM/scanning near-field optical microscope (SNOM; Nanonics Imaging Ltd.). A schematic of the SNOM setup is shown in Figure 1. We used a He−Cd laser operating at 442 nm as the illumination

* Corresponding author. E-mail: ctistis@caesar.de. Address: Caesar Research Center, Nanoparticle Technology Department, Ludwig-Erhard-Allee 2, 53175 Bonn, Germany.
† Center of Advanced Studies and Research.
‡ Boston College.

10.1021/nl0712973 CCC: $37.00
Published on Web 08/23/2007

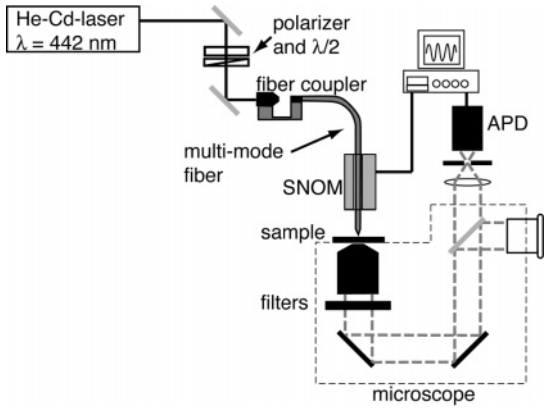

Figure 1. Schematic of the experimental setup for the illumination-mode SNOM measurements in transmission.

source. After passing a half-wave plate and a polarizer, enabling us to control intensity as well as polarization, the light was coupled into a multimode fiber with a tapered Al-coated tip. The aperture diameter of the fiber tip was between 50 and 100 nm, offering us the opportunity to locally illuminate the sample. Working in transmission mode, the light was collected behind the sample through a microscope and, after letting it pass a filter, it was directed to an avalanche photodiode.

Results and Discussion. The film materials were chosen for their different electronic and, consequently, their different optical properties. Gold is a high-conductive noble metal with strong d−s interband transitions and a well-pronounced bulk plasmon excitation, strongly contributing to the optical response in the visible.[28] Aluminum, on the other hand, is a high-conductive free-electron metal (only a weak interband absorption in the visible) with the bulk and regular surface plasmon excitations in the far-UV range.[29] Typical transmission spectra of the different samples, covering a range of wavelengths between 200 and 2500 nm, are shown in Figure 2a for the gold and Figure 2b for the aluminum films, respectively. The influence of the sapphire substrate has been subtracted by taking a spectrum of the bare substrate as reference. Both graphs also include the spectra of solid 20 nm thick films (black lines) for comparison. The hole diameter is 250 nm, and the interhole distance 470 nm.

The solid gold film (black line, Figure 2a) shows the expected spectral features with a strong peak due to d−p interband transition at 2.5 eV. This can also be seen in the spectra of the perforated films (open symbols). A significant number of additional spectral features are visible for the gold arrays with holes. These additional peaks also show a red-shift as well as a broadening with decreasing film thickness. The most interesting features are the two pronounced ones in the strong subwavelength regime, above 1000 nm wavelength (the holes are 250 nm in diameter): one at 1200 nm and the other at 2100 nm, respectively. With decreasing film thickness, these features seem to exchange their oscillator strengths and, for the 20 nm film, only the first, strongly enhanced peak survives. Such oscillator-strength exchange is typical of mode anticrossing. Corresponding subwavelength features are absent in the perforated aluminum films.

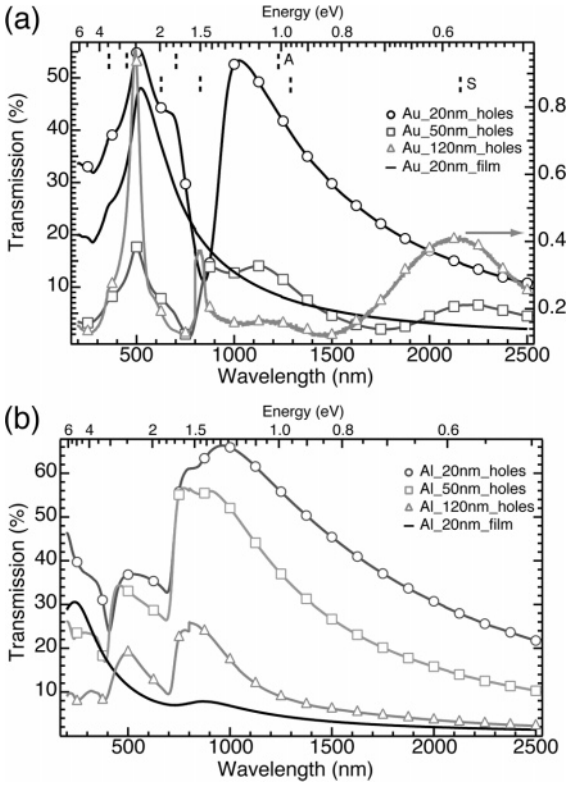

Figure 2. UV−vis transmission spectra: (a) Gold film with a thickness of 20 nm (black line) as well as three films with hole arrays. The film thickness varies between 20 and 120 nm, respectively (open symbols), showing differences in their spectral features. (b) Aluminum film with a thickness of 20 nm (black line) and the hole array Al films with thicknesses between 20 and 120 nm, respectively (open symbols).

All the additional (hole related) features can be attributed to surface plasmons (SP) and Wood anomalies[18−20,30] due to the periodicity of and the coupling of the light to the array. Considering only zero-order transmission, the coupling of the light to the grating obeys the conservation of momentum $\vec{k}_{SP} = \vec{K}_0 + i\vec{b}_x + j\vec{b}_y$, where the in-plane projected component of the light wave vector $\vec{k}_0$ is $\vec{K}_0 = (\omega/c)(\vec{k}_0/|\vec{k}_0|) \sin \vartheta$, with ω the light's frequency, c the speed of light, $\vec{b}_x$ and $\vec{b}_y$ the reciprocal unit vectors for a hexagonal lattice, ϑ the incident angle of the light, and i and j integers. The equation of the eigenmodes of a single planar metal−dielectric interface is given by:[31]

$$|\vec{k}_{SP}| = \frac{\omega}{c}\sqrt{\frac{\epsilon_m \epsilon_d}{\epsilon_m + \epsilon_d}} \qquad (1)$$

with ϵ_m the real part of the dielectric constant of the metal and ϵ_d the dielectric constant of the dielectric. Combining eq 1 with the conservation of momentum, SP resonances are expected at wavelengths:[31]

$$\lambda = \frac{a_0}{\sqrt{\frac{3}{4}(i^2 + j^2 + ij)}}\sqrt{\frac{\epsilon_m \epsilon_d}{\epsilon_m + \epsilon_d}} \qquad (2)$$

with a_0 the periodicity of the array and the integers i and j denoting the order of the SP resonances. Because we have asymmetric conditions, i.e., air on one side and sapphire on the other side of the metallic hole array, the expected wavelengths have to be calculated for each interfaces. The peak positions for gold using eq 2 are indicated by dotted lines in Figure 2a. The upper line, denoted by A, shows the peak positions for the metal−air interface, while the lower line, denoted by S, gives the positions for the metal−sapphire interface.

These considerations explain the features above 500 nm in the case of the two thicker gold hole arrays (Figure 2a, open triangles and squares), including the two features in the strongly subwavelength regime, discussed above. At the wavelength region of the bulk plasmon, at around 500 nm (2.5 eV), the transmission is totally intermixed with Wood-anomaly-related peaks, creating a complex pattern. Because this very simple single-interface-at-a-time approach is justified only for films that are much thicker than the field penetration depth (∼20 nm), some discrepancy is expected for the 20 nm film. For this very thin film, a direct transmission strongly contributes as well.

The origin of the aforementioned peak-shift is probably an effect of the aspect ratio of the holes and the resulting strength of the coupling of the surface plasmons on both sides of the metal film, being in agreement with experiments for thick films.[32] For a more thorough understanding of this peak-shift in the thin-film regime, experiments are currently in preparation.

Figure 2b shows the spectra for the aluminum. Again, the black line displays the spectrum for a 20 nm thick solid film, showing the known interband transition at 800 nm (1.5 eV). Unlike the spectra for the gold hole arrays, the spectra for the perforated films of aluminum are essentially identical for the different thicknesses, except for the overall scaling. The peaks at 800 nm are due to the interband transition still persist, but in contrast to the case of gold, there are no features in the strongly subwavelength regime, i.e., for wavelengths greater than 1000 nm. The features below 700 nm are most likely due to Wood anomalies. The minimum near 400 nm has a Fano profile, pointing toward Wood anomalies mediated by surface plasmons.

After the far-field characterization of the metallic hole arrays, we studied the near-field optical behavior of the light transmission to determine the major transmission channel for the light through the film. The experiments were performed in illumination mode, giving us the opportunity to locally illuminate the sample using a wavelength of 442 nm. Figure 3 shows the results for the three gold arrays with a thickness of 20 nm (Figure 3a,b), 50 nm (Figure 3c,d), and 120 nm (Figure 3e,f), respectively, the hole diameter being 250 nm. Thereby, the pictures of the topographic (left column) and the optic signal (right column) were taken simultaneously. By comparing the topography with the optical signal, the measurements reveal a high transmission at the position of the holes for all thicknesses. This observed contrast might be explained by the direct light transmission through these marginally subwavelength holes, enhanced by

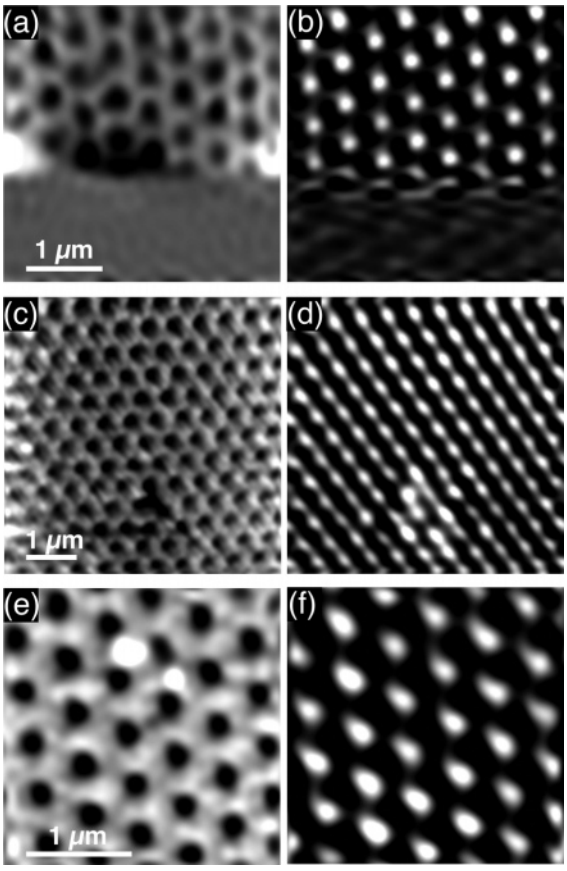

Figure 3. SNOM images of the hole arrays in the Au films. Left column: Topography images of the samples indicating an interhole distance of ∼500 nm and a hole diameter of 250 nm. Right column: Near-field optical images taken at a wavelength of 442 nm. The recorded light intensity shows an enhanced transmission through the subwavelength holes. The thickness of the deposited films is 20 nm (a,b), 50 nm (c,d), and 120 nm (e,f), respectively.

the excitation of surface plasmons. A closer look at the optical images reveals an elongation of the circular holes. This is not a tip artifact but the result of the incoming light polarization. The elongation is parallel to the direction of the polarization[33] and indicates coupling to surface plasmons. A strong demonstration of this is shown in Figure 3d, where a higher transmission is not only observed at the position of the holes but also in between them, in the direction of the polarization.

Because the films are optically thin, the contrast of the optical pictures in Figure 3 had to be enhanced to make the enhanced transmission visible. To show that the interpretation of the contrast is correct, a scratch in a 100 nm thick Au film was measured (Figure 4). Here, only the optical image is shown. On the left-hand side of the picture, the gold film has been removed and the bare sapphire substrate is visible. The line indicates the position of the scan shown in the graph at the right-hand side. The black line shows the topographic signal where the step of the scratch is visible. The gray line indicates the optical image. One can see that, on the left-hand side, the optical signal is stronger than that on the side with the film. The large intensity enhancement at the border is an artifact of the measurement technique. Comparing the position of the intensity maxima with the position of the holes

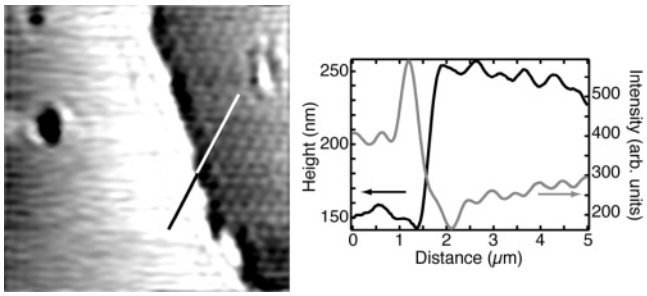

Figure 4. SNOM image of a scratch in the hole array of the 100 nm thick Au film. The measured contrast indicates a light transmission through the holes. This is confirmed by the line scan given on the right. The maxima in optical transmission fall into the minima of the topography signal.

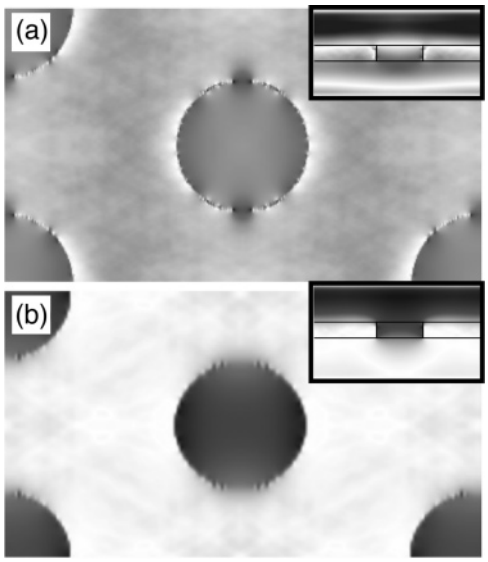

Figure 5. Simulation of the light transmission through the Au film with an array of holes. Parameters: interhole distance: 500 nm, hole diameter 250 nm, film thickness 50 nm, wavelength of the light is 442 nm (a) and 1000 nm (b). Main figures show light intensity 10 nm away from the film surface on the far side. Darker regions represent higher intensity. Insets show the corresponding in-plane electric field amplitudes.

(minima in the topographic signal), our interpretation of the contrast in Figure 3 is confirmed because the intensity maxima lie at the position of the holes.

For a more thorough understanding of the underlying physical processes, we used a 3D finite-difference time-domain (FDTD)[34] numerical simulation to model the transmitted field distributions. We used periodic boundary conditions associated with the hexagonal hole structure and absorption conditions to truncate the directions parallel to the film surface. The thickness of the film was taken to be 50 nm, the interhole distance is 500 nm, and the diameter $d = 250$ nm, as in the experiment. The discretization step size of 2 nm assures good numerical convergence. The time-domain auxiliary differential equation approach was used to implement the FDTD method to our case of the dispersive metal. The frequency-dependent permittivity of Au was taken from ref 35. The in-plane field intensity profiles shown in Figure 5 are calculated in a single unit cell, at 10 nm away from the film surface, on the far side of the film. The chosen

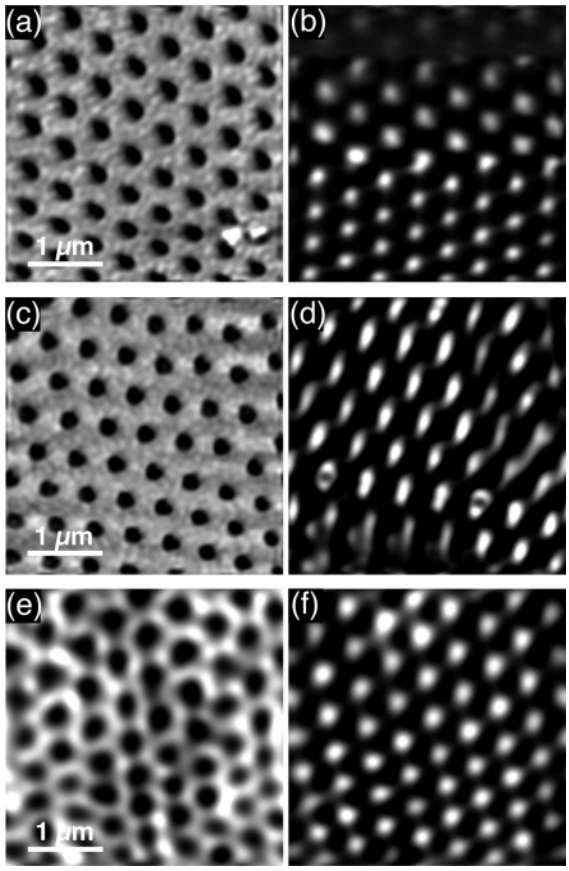

Figure 6. SNOM images of the hole arrays in the Al films. Left column: Topography images of the samples indicating an interhole distance of ~500 nm and a hole diameter of 250 nm. Right column: Near-field optical images at a wavelength of 442 nm. The recorded light intensity again shows an enhanced transmission through the subwavelength holes. The thicknesses of the deposited films are 20 nm (a,b), 50 nm (c,d), and 120 nm (e,f), respectively.

color-coding scheme shows high-intensity regions as a darker color. The light wavelength is $\lambda = 442$ nm in Figure 5a, and $\lambda = 1000$ nm in Figure 5b. The insets show the corresponding in-plane electric field amplitude profiles across the film. In the marginal subwavelength regime ($d < \lambda$, Figure 5a), the overall transmission of light through the film and holes is very high (largely due to the plasmon enhancement), as shown in the inset. The corresponding in-plane intensity map shows that the transmission is larger in the holes, in agreement with the experiment. In the strongly subwavelength regime ($d \ll \lambda$, Figure 5b), the light propagation through metal is marginal (in part because little plasmon enhancement occurs in this range) but is quite large through the holes. This is obvious from the inset, as well as, the corresponding in-plane intensity map. An overall transmission coefficient through this film is at this wavelength ($\lambda = 1000$ nm), much smaller than that for $\lambda = 442$ nm, as evidenced by the insets in Figure 5a,b. A maximum in transmission coefficient is indeed observed at $\lambda = 442$ nm in all curves in Figure 2a, followed by a smaller, much broader maximum at $\lambda = 1000$ nm.

For a better comparison, we had studied the near-field optical transmission through aluminum films with the same thickness as the gold films, i.e., 20 nm (Figure 6a,b), 50 nm

(Figure 6c,d), and 120 nm (Figure 6e,f). As before, the left column represents the topographic signal and the right column the simultaneously measured optic signal.

As in the case of gold, the observed contrast shows an enhanced transmission of light through the holes and is the result of a direct photon penetration through these, only marginally subwavelength holes, with a possible surface plasmon enhancement. Even though aluminum is considered a nonplasmonic metal in the visible range, surface plasmon polaritons, or "spoof plasmons" (coupled photon−plasmon modes), could be generated.[36] Whether the native oxide layer has an influence on the transmission properties of the hole array could not be clarified. Further experiments and calculations with regard to this are being prepared.

Summary and Outlook. In our experiments, we were able to show that the transmission of the light through a hexagonal array of subwavelength holes in a metallic film is highly dependent on the optical properties of the metal. The transmission is governed by surface plasmons and Wood anomalies, which determine the position of the transmission maxima. Our near-field measurements showed that, although the films were optically thin and despite the huge background, it was possible to identify the propagation path of the light. We clearly saw a plasmon-assisted enhanced transmission through the subwavelength holes, which is in excellent agreement with our theoretical calculations.

Further investigations concerning the wavelength dependence of the transmission in the near field as well as the dependence on the hole diameter and interhole distance are currently being prepared.

Acknowledgment. We thank F. J. García de Abajo for many fruitful discussions and W. Kandulski for his advice in the preparation of the metallic hole arrays. M. Giersig thanks the Fulbright Commission for the Fellowship at Boston College and Harvard University. We acknowledge the financial support of the Deutsche Forschungsgemeinschaft through grant no. SP53-100.

References

(1) Bethe, H. A. *Phys. Rev.* **1944**, *66*, 163.
(2) Levine, H.; Schwinger, J. *Phys. Rev.* **1948**, *74*, 958.
(3) Bouwkamp, C. J. *Philips Res. Rep.* **1950**, *5*, 321; Bouwkamp, C. J. *Rep. Prog. Phys.* **1954**, *17*, 35.
(4) Dürig, U.; Pohl, D. W.; Rohner, F. *J. Appl. Phys.* **1986**, *59*, 3318.
(5) Andrews, C. L. *Phys. Rev.* **1947**, *71*, 777.
(6) Ehrlich, M. J.; Silver, S.; Held, G. *J. Appl. Phys.* **1955**, *65*, 336.
(7) Kolb, G.; Karrai, K.; Abstreiter, G. *Appl. Phys. Lett.* **1994**, *65*, 3090.
(8) Ctistis, G.; Schimek, O.; Fumagalli, P.; Paggel, J. J. *J. Appl. Phys.* **2006**, *99*, 014505.
(9) Ebbesen, T. W.; Lezec, H. J.; Ghaemi, H. F.; Thio, T.; Wolff, P. A. *Nature* **1998**, *391*, 667.
(10) Martín-Moreno, L.; García-Vidal, F. J.; Lezec, H. J.; Pellerin, K. M.; Thio, T.; Pendry, J. B.; Ebbesen, T. W. *Phys. Rev. Lett.* **2001**, *86*, 1114.
(11) Bonod, N.; Enoch, S.; Li, L.; Popov, E.; Nevière, M. *Opt. Express* **2003**, *11*, 482.
(12) Lezec, H. J.; Thio, T. *Opt. Express* **2004**, *12*, 3629.
(13) Genet, C.; van Exeter, M. P.; Woerdman, J. P. *J. Opt. Soc. Am. A* **2005**, *22*, 998.
(14) Genet, C.; van Exeter, M. P.; Woerdman, J. P. *Opt. Commun.* **2003**, *225*, 331.
(15) Salomon, L.; Grillot, F.; Zayats, A. V.; de Fornel, F. *Phys. Rev. Lett.* **2001**, *86*, 1110.
(16) Sarrazin, M.; Vigneron, J.-P.; Vigoureux, J.-M. *Phys. Rev. B* **2003**, *67*, 085415.
(17) Kretschmann, M.; Maradudin, A. A. *Phys. Rev. B* **2002**, *66*, 245408.
(18) Ghaemi, H. F.; Thio, T.; Grupp, D. E.; Ebbesen, T. W.; Lezec, H. J. *Phys. Rev. B* **1998**, *58*, 6779.
(19) Kim, T. J.; Thio, T.; Ebbesen, T. W.; Grupp, D. E.; Lezec, H. J. *Opt. Lett.* **1999**, *24*, 256.
(20) Krishnan, A.; Thio, T.; Kim, T. J.; Lezec, H. J.; Ebbesen, T. W.; Wolff, P. A.; Pendry, J.; Martin-Moreno, L.; Garcia-Vidal, F. J. *Opt. Commun.* **2001**, *200*, 1.
(21) Gao, H.; Henzie, J.; Odom, T. W. *Nano Lett.* **2006**, *6*, 2104.
(22) Beermann, J.; Bozhevolnyi, S. I. *Laser Phys. Lett.* **2004**, *1*, 592.
(23) Kim, J. H.; Moyer, P. J. *Opt. Express* **2006**, *14*, 6595.
(24) Klein Koerkamp, K. J.; Enoch, S.; Segerink, F. B.; van Hulst, N. F.; Kuipers, L. *Phys. Rev. Lett.* **2004**, *92*, 183901.
(25) Genet, C.; Ebbesen, T. W. *Nature* **2007**, *445*, 39.
(26) Maier, S. A.; Atwater, H. A. *J. Appl. Phys.* **2005**, *98*, 011101.
(27) Kosiorek, A.; Kandulski, W.; Chudzinski, P.; Kempa, K.; Giersig, M. *Nano Lett.* **2004**, *4*, 1359. Kosiorek, A.; Kandulski, W.; Glaczynska, H.; Giersig, M. *Small* **2005**, *1*, 439.
(28) Sommers, C. B.; Amer, H. *Phys. Rev.* **1969**, *188*, 1117. Ramchandani, M. G. *J. Phys. C* **1970**, *3*, S1.
(29) Segall, B. *Phys. Rev.* **1961**, *124*, 1797. Brust, D. *Solid State Commun.* **1970**, *8*, 413.
(30) Wood, R. W. *Philos. Mag.* **1902**, *4*, 396. Wood, R. W. *Phys. Rev.* **1935**, *48*, 928.
(31) Raether, H. *Surface Plasmons*; Springer-Verlag: Berlin, 1998.
(32) Degiron, A.; Lezec, H. J.; Barnes, W. L.; Ebbesen, T. W. *Appl. Phys. Lett.* **2002**, *81*, 4327.
(33) Sönnichsen, C.; Duch, A. C.; Steininger, G.; Koch, M.; von Plessen, G. *Appl. Phys. Lett.* **2000**, *76*, 140.
(34) Taflove, A. *Computational Electrodynamics: The Finite-Difference Time-Domain Method*, 2nd ed.; Artech House: Norwood, MA, 2000.
(35) Palik, E. D. *Handbook of Optical Constants in Solids*; Academic Press: Boston, 1991; Vol. 1.
(36) Pendry, J. B.; Martin-Moreno, L.; Garcia-Vidal, F. J. *Science* **2004**, *305*, 847.

NL0712973